# Creation of graphic database specifying android arm mechanism work envelope taking into account forbidden zones position

**F N Pritykin[1] and V I Nebritov [1]**

[1] Omsk State Technical University, 11, Mira ave., Omsk, 644050, Russia

E-mail: pritykin@mail.ru

**Abstract.** The structure of graphic database specifying the shape and the work envelope projection position of an android arm mechanism with various positions of the known in advance forbidden zones is proposed. The technique of analytical assignment of the work envelope based on the methods of analytical geometry and theory of sets is represented. The conducted studies can be applied in creation of knowledge bases for intellectual systems of android control functioning independently in the sophisticated environment.

## 1. Introduction

Creating universal algorithms for examination of manipulator mechanism functionality is still a topical problem [1-4]. In this respect 3D development of the virtual environment to model experiments to analyze the behavior of independently functioning androids in organized environments is one of the important problems of robotics [5-7]. The solution to the specified problem is inter-related with work envelope construction of the robot arm mechanism taking into account the known in advance environment. An analytical assignment of the work envelope allows analyzing goals position of the synthesized trajectory for the output link and defining their attainability at the initial stage of arm motion realization [8-9]. The most frequent motional task for an android is putting a working object on or taking it off the tool rack. Therefore let us examine the influence of the forbidden zones on the work envelope of android arm mechanism, these zones being the tool racks of different height.

## 2. Problem statement

In Figure 1 the images of android AR-600E arm mechanism kinematic diagram and forbidden zones $P_1$ and $P_2$ are shown. These forbidden zones specify the position of tool-racks $P_1$ and $P_2$. The figure illustrates the virtual safe zone of $l_\delta$ = 50mm in thickness around obstacles. In the course of experiments this zone proves to be forbidden, the intersection of arm configuration and this zone as a result of a calculation error not resulting in the damage of mechanism or working objects and tool-racks. In Figure 1 points $O_1$, $O_2$ and so on define the origin of coordinates used for assignment of a kinematic chain model. The values of generalized coordinates assigned by the vector $\boldsymbol{q}$ ($q_1$, …, $q_5$) (Fig. 1) are varied within the specified range and defined by the inequalities:

$$q_i^{min} \le q_i \le q_i^{max} \quad (1)$$

where $q_i^{min}$, $q_i^{max}$ are the innermost and outermost limits of generalized coordinates. In the considered example the specified values are equal to $q_i^{min}$ (-10°, -100°, -90°, -120°, -120°) and $q_i^{max}$ (10°, 120°, 120°, 120°, 120°) respectively. The parameters $x_t$ and $x_{11}$ in Figure 1 then define the assigned safe

distance between the body and the tool-racks and minimum permissible value of the coordinate $x_{11}$ specifying the center $O_{11}$ of the output link (OL). The coordinates $x_{B1}$ and $z_{B1}$ specify the position of the reference point $B_1$ of the forbidden zone $P_1$.

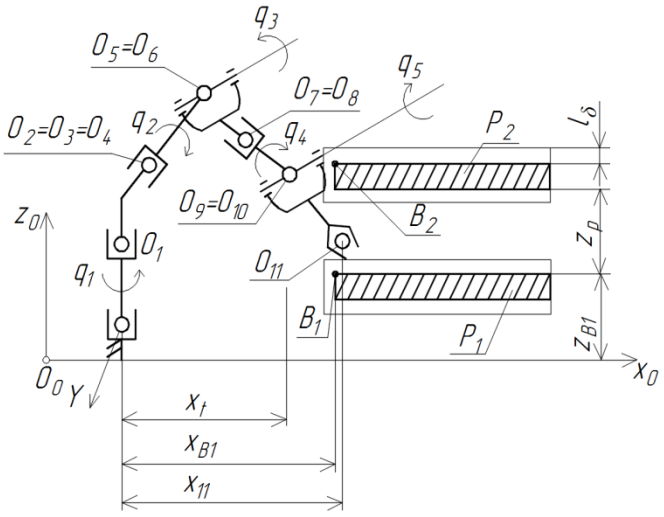


**Figure 1.** Relative position of the android arm mechanism and tool-racks.

Let us construct the set of gripping centers positions (possible positions of point $O_{11}$) defining the work envelope of an android arm mechanism provided the intersection of the arm configuration and forbidden zones is absent. Let the alteration in pitch of generalized coordinates $\Delta q_i$ be equal to 5° in construction of the work envelope.

**3. Computational results for the work envelop projection of android arm mechanism with forbidden zones taken into account**

The block diagram in Figure 2 represents the construction of OL center (point $O_{11}$) positions set of the work envelope.

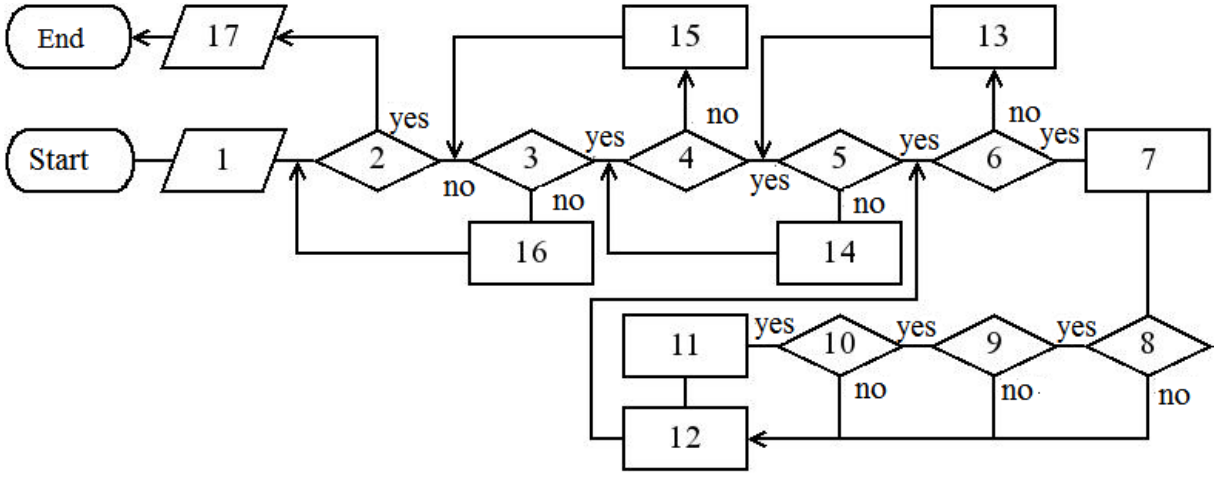


**Figure2.** The algorithm of points construction of android arm mechanism work envelope taking the position of forbidden zones $P_1$ and $P_2$ into account.

The following notation is introduced in Figure 2: 1 – data input, $n$, $q_i^{min}$, $q_i^{max}$, $\Delta q_i$, $x_{11}^{min}$, $x_{B1}$, $z_{B1}$, $x_{B2}$, $z_{B2}$ and $z_P$; 2 – condition test $q_1 < q_1^{max}$; 3 – $q_2 < q_2^{max}$; 4 – $q_3 < q_3^{max}$; 5 – $q_4 < q_4^{max}$; 6 – $q_5 < q_5^{max}$; 7 – calculation $p_1 = 0$ if $q_i > q_i^{max}$, if not $p_1 = 1$, calculation $p_2 = 0$ in case the intersection of the arm

configuration and the obstacle is absent, if not $p_2 = 1$; 8 – condition test $p_1 = 0$ (if values of $q_i$ satisfy the limit values of generalized coordinates); 9 – condition test $p_2 = 0$ (the condition of the configuration and the obstacle intersection); 10 – $x_{11} > x_{11}^{min}$ (where $x_{11}^{min}$ — assigned minimum permissible values of the coordinate $x_{11}$, in the considered example $x_{11}^{min} = 400$ mm); 11 – Point belongs to the section of the working region. Imaging the given point; 12 – $q_5 = q_5 + \Delta q_i$; 13 – $q_4 = q_4 + \Delta q_i$, $q_5 = q_5^{min}$; 14 – $q_3 = q_3 + \Delta q_i$, $q_4 = q_4^{min}$, $q_5 = q_5^{min}$; 15 – $q_2 = q_2 + \Delta q_i$, $q_3 = q_3^{min}$, $q_4 = q_4^{min}$, $q_5 = q_5^{min}$; 16 – $q_1 = q_1 + \Delta q_i$, $q_2 = q_2^{min}$, $q_3 = q_3^{min}$, $q_4 = q_4^{min}$, $q_5 = q_5^{min}$; 17 – array extraction of point data belonging to the section of the work envelope.

Figure 3abc shows an image of the work envelope for accordingly specified values $z_{B1} = 350$ mm, $z_{B1} = 200$ mm and $z_{B1} = 500$ mm at $x_{B1} = 400$ mm. The parameter $z_p$ is set to be 100 mm. Figure 3d presents the top view of the work envelope being the same for all three represented versions of the work envelope in Figure 3abc. The work envelope is designed for the configurations of the arm not intersecting the forbidden zones $P_1$ and $P_2$ and being located at the safe distance of $l_\delta < 50$ mm.

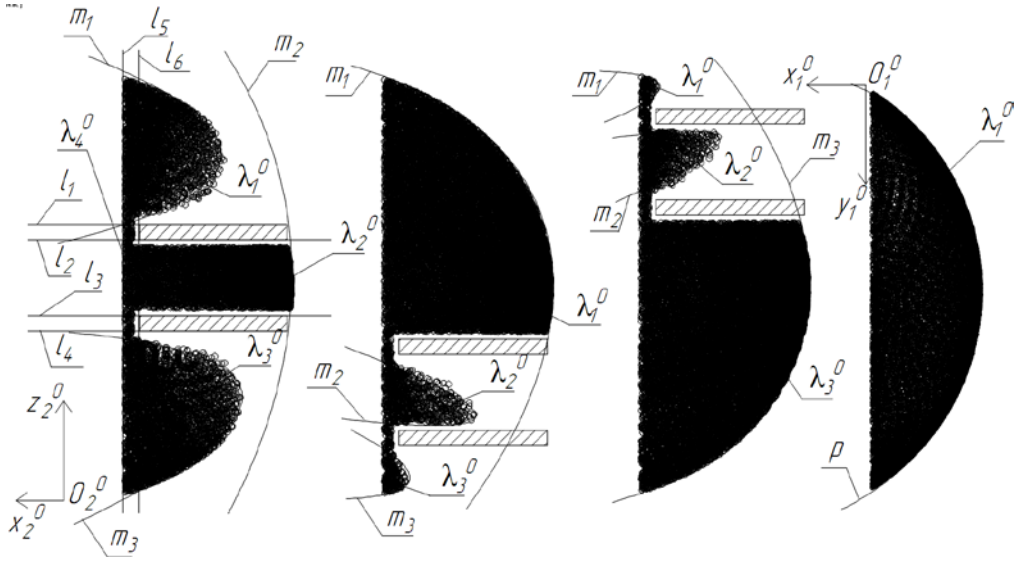


**Figure 3.** Representation of the work envelope with the tool-racks position on the elevation and top views being taken into account when $x_{B1} = 400$ mm: (a) – $z_{B1} = 1200$ mm; (b) – $z_{B1} = 1350$ mm; (c) – $z_{B1} = 1500$ mm; (d) – representation of the work envelope on the top view.

As the figure indicates the specified graphic images of top views are defined with six lines $l_i$ and three second-order curves that is parabolas $m_i$. The parabolas are most accurately fit the contours of the work envelop. The work envelop contour on the top view is assigned by the radial arc $p$.

## 4. Analytical assignment of the work envelop projection contours

Mathematical models of graphic images $\lambda^0_i$ for the work envelop projection regions are defined based on theory of sets [9]. Lines $l_i$ position data and parabolas $m_i$ position and shape are prescribed by algebraic equations coefficients for these graphic objects in the inertial system with the graphic data base depending on the values of $z_B$ and $z_P$.

To define the goals belonging to the work envelop let us assign this envelop with the theory of sets, these goals prescribing the end position of the OL center on synthesized trajectories [9]. The work envelop is defined as the intersection of regions $\Delta_1, \Delta_2, \ldots \Delta_9$ on the elevation view.

The regions $\Delta_{1\text{-}6}$ (assigned by the lines $l_1 – l_6$ on the elevation view) are defined by inequalities of the form (Fig. 3abc):

$$-x^0\left(z_{i-1}^0 - z_i^0\right) + z^0\left(x_{i-1}^0 - x_i^0\right) - x_{i-1}^0 \cdot z_i^0 + x_i^0 \cdot z_{i-1}^0 \geq 0\,, \tag{2}$$

or

$$A_i\, x^o + B_i\, y^o + C_i \geq 0, \tag{3}$$

where $x_i^0$, $z_i^0$ and $x^0_{i-1}$, $z^0_{i-1}$ are the point coordinates wherethrough lines $l_1 - l_6$ are drawn, $x^0$, $z^0$ are the coordinates of the current point line respectively.
The three regions on the elevation view $\Delta_7$, $\Delta_8$ and $\Delta_9$ are defined by the parabolic curves $m_1$, $m_2$ and $m_3$ (Fig. 3abc). The points assigning inequalities within the regions $\Delta_{7\text{-}9}$ appear as follows:

$$\begin{aligned}
&\left(x_0\cos\varphi^{\Delta 7} + z_0\sin\varphi^{\Delta 7} + m_x^{\Delta 7}\right)^2 - 2p^{\Delta 7}\left(x_0\sin\varphi^{\Delta 7} + z_0\cos\varphi^{\Delta 7} + m_z^{\Delta 7}\right) \geq 0,\\
&\left(x_0\cos\varphi^{\Delta 8} + z_0\sin\varphi^{\Delta 8} + m_x^{\Delta 8}\right)^2 - 2p^{\Delta 8}\left(x_0\sin\varphi^{\Delta 8} + z_0\cos\varphi^{\Delta 8} + m_z^{\Delta 8}\right) \geq 0,\\
&\left(x_0\cos\varphi^{\Delta 9} + z_0\sin\varphi^{\Delta 9} + m_x^{\Delta 9}\right)^2 - 2p^{\Delta 9}\left(x_0\sin\varphi^{\Delta 9} + z_0\cos\varphi^{\Delta 9} + m_z^{\Delta 9}\right) \geq 0,
\end{aligned} \tag{4}$$

where $m_x^{\Delta 7}$, $m_y^{\Delta 7}$, $p^{\Delta 7}$, $\varphi^{\Delta 7}$ and so on define the form and position parameters of the curves $m_1$, $m_2$ and $m_3$ determining points within the regions $\Delta_{7\text{-}9}$ (Fig. 4ab). The parameters $m_x^{\Delta 8}$, $m_y^{\Delta 8}$ in Figure 4 define the center of the coordinate system $O'x'z'$ connected with the parabola. The parabola point has the coordinate $z' = 0$ (Fig. 4ab). The parameter $\varphi^{\Delta 8}$ assigns the inclination angle of the axis $x'$ determining the parabola inclination to the axis $x^o$. The value $p^{\Delta 8}$ prescribes a focus point of parabola. The inequalities (4) are obtained by transforms of coordinates assigning the transition from the system $O'x'z'$ to the system $O^0x^0z^0$ (Fig. 4ab). Figure 4ab shows the position of the three lines $l_2$, $l_3$, $l_6$, the curve $m_2$ and the region $\lambda_2^0$ resulted from the intersection of regions $\Delta_2$, $\Delta_3$, $\Delta_6$ and $\Delta_8$ with parameters $z_{B1}$ = 500 mm, $z_{B1}$ = 350 mm and $x_{B1}$ = 400 mm.

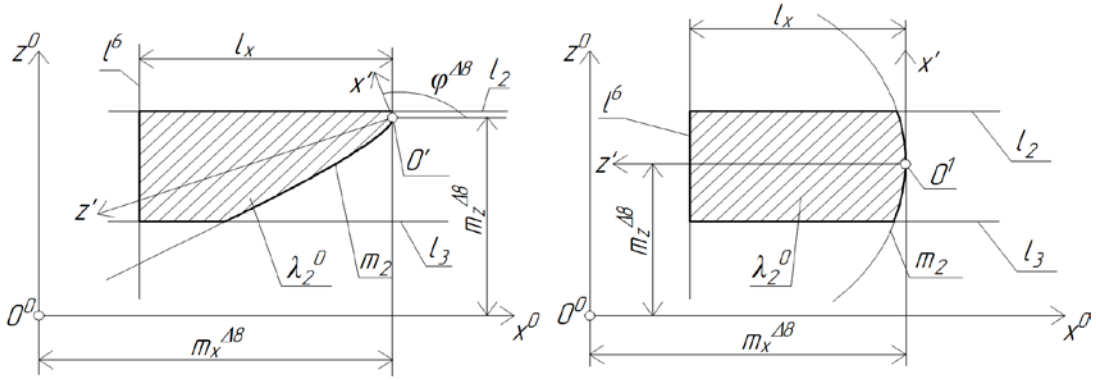


**Figure 4.** Different versions of analytical assignment of the region $\lambda_2^0$ of the android arm mechanism work envelop fragment on the elevation view at: a) – $z_{B1}$ = 500 mm, $x_{B1}$ = 400 mm; (б) – $z_{B1}$ = 350 mm, $x_{B1}$ = 400 mm.

In Figure 4 the value of the parameter $l_x$ defines the outermost point of region $\lambda_2^0$ of the work envelop fragment from the line $l_6$. The intersection of regions is performed with the operations of Boolean algebra [9]:

$$\begin{aligned}\lambda_1^0 &= \Delta_5 \cap \Delta_7,\\ \lambda_2^0 &= \left(\left(\Delta_2 \cap \Delta_3\right) \cap \Delta_6\right) \cap \Delta_8,\\ \lambda_3^0 &= \Delta_5 \cap \Delta_9,\\ \lambda_4^0 &= \left(\left(\Delta_5 \cap \Delta_6\right) \cap \Delta_1\right) \cap \Delta_4.\end{aligned} \tag{5}$$

The set of R-functions reflecting the logic of work envelops projection graphic imaging (5) is also predetermined in the array, based on regions $\Delta_i$ these envelops are defined by the lines $l_1$ - $l_6$, parabolas $m_1$ - $m_3$ and curve $p$.. The graphic database structure fragment is shown in Tables 1 and 2.

**Table 1.** Coefficients values of lines $l_1 \div l_6$ equations.

| $z_p$ | $z_B$ | $l_1$ | | | $l_2$ | | | $l_3$ | | |
|---|---|---|---|---|---|---|---|---|---|---|
| *mm* | *mm* | $A_1$ | $B_1$ | $C_1$ | $A_2$ | $B_2$ | $C_2$ | $A_3$ | $B_3$ | $C_3$ |
| 100 | 1200 | 0 | -210 | 69300 | 0 | -210 | 60900 | 0 | -210 | 48300 |
| | 1500 | 0 | -210 | 132300 | 0 | -210 | 123900 | 0 | -210 | 111300 |
| $z_p$ | $z_B$ | $l_4$ | | | $l_5$ | | | $l_6$ | | |
| *mm* | *mm* | $A_4$ | $B_4$ | $C_4$ | $A_5$ | $B_5$ | $C_5$ | $A_6$ | $B_6$ | $C_6$ |
| 100 | 1200 | 0 | -210 | 39900 | -80 | 0 | 28000 | -80 | 0 | 31200 |
| | 1500 | 0 | -210 | 102900 | -80 | 0 | 28000 | -80 | 0 | 31200 |

**Table 2**. Coefficients values of parabolas $m_1 \div m_3$ equations.

| $z_p$ | $z_B$ | $m_1$ | | | | $m_2$ | | | | $m_3$ | | | |
|---|---|---|---|---|---|---|---|---|---|---|---|---|---|
| *mm* | *mm* | $m_x^{\Delta 7}$ | $m_y^{\Delta 7}$ | $\varphi^{\Delta 7}$ | $p^{\Delta 7}$ | $m_x^{\Delta 8}$ | $m_y^{\Delta 8}$ | $\varphi^{\Delta 8}$ | $p^{\Delta 8}$ | $m_x^{\Delta 9}$ | $m_y^{\Delta 9}$ | $\varphi^{\Delta 9}$ | $p^{\Delta 9}$ |
| 100 | 1200 | 622 | 1535 | 108 | 249.4 | 510 | 1212 | 73 | 2.64 | 432 | 1136 | 77 | 3.61 |
| | 1500 | 413 | 1755 | 111 | 2.69 | 494 | 1572 | 63 | 2.55 | 627 | 1524 | 73 | 251.1 |

## 5. Conclusion

In Figure 5 the results of movements synthesis along the velocity vector [8] using the graphic database with a focus on working object transfer from the point $A^н$ to the point $A^к$ are presented. The points $A^н$ and $A^к$ in the figure are specified by the projections $A_1{}^н$ , $A_2{}^н$, $A_1{}^к$ and $A_2{}^к$. At the initial stage of android motion virtual modeling the algorithm defines the goal $A^к$ membership in the region $\lambda_2{}^0$ (Fig. 3abc). If a specified point is in the region $\lambda_2{}^0$, motion synthesis is performed in specified trajectory sections along the velocity vector.

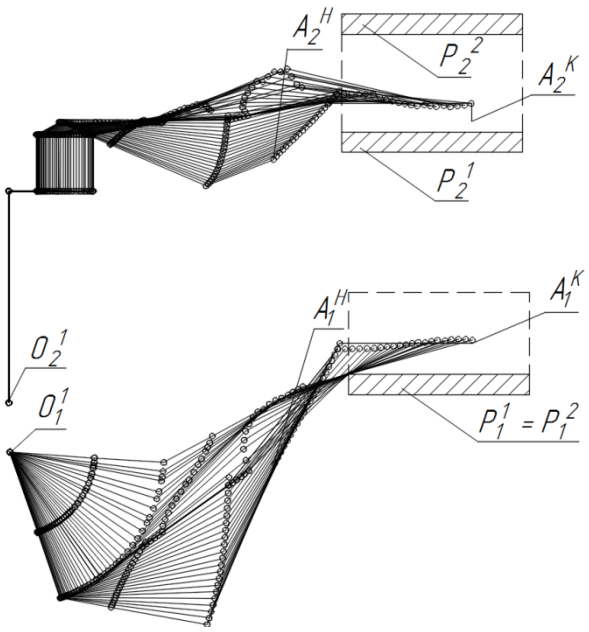


**Figure 5.** The result of motion synthesis to the end point of the synthesized trajectory.

The results of computational experiments demonstrate the calculation time reduction for tests related to putting a working object on or taking it off the tool rack with the use of the developed graphic databases. The presented research results can be applied in virtual modeling of an android motion in the known in advance sophisticated environment.

## References

[1] Pratt J, Dilworth P and Pratt G 1997 Virtual model control of a bipedal walking robot *Proceedings of Int. Conf. on Robotics and Automation* 1 pp 193–198
[2] You B, Zou Y, Xiao W and Wang J 2010 Telerobot control system based on dual-virtual model and virtual force *Int. Forum on Strategic Technology* pp 246–250
[3] Hrr J, Pratt J, Chew C-M, Herr H and Pratt G 1998 Adaptive virtual model control of a bipedal walking robot *Proceedings of Int. Joint Symp. on Intelligence and Systems* pp 245–251
[4] Tsukamoto H K, Takubo T, Ohara K, Mae Y and Arai T 2010 Virtual impedance model for obstacle avoidance in a limb mechanism robot *Int. Conf. on Information and Automation* pp 729-734
[5] Hasegawa T, Suehiro T and Takase K 1992 A model-based manipulation system with skill-based execution *IEEE Transactions on Robotics and Automation* **8** pp 535–544
[6] Hrr J, Pratt J, Chew C, Herr H and Pratt G 1998 Adaptive virtual model control of a bipedal walking robot *IEEE Int. Simp. Intellegence and Systems* pp 245–251
[7] Lopatin P 2016 Investigation of a Target Reachability by a Manipulator in an Unknown Environment *IEEE International Conference on Mechatronics and Automation* pp 37–42
[8] Pritykin F N and Tevlin A M 1987 Procedure for construction of manipulator motions from a given local grip path in the presence of obstacles *Soviet machine science* **4** pp 30–33
[9] Rvachev V L 1974 Methods of Logic Algebra in Mathematical Physics (Kiev) 256